Measurement of dye diffusion in scattering tissue phantoms using dual-wavelength low-coherence interferometry

Trude Støren
Norwegian University of Science and Technology
Department of Physics
N-7491 Trondheim, Norway

Arne Røyset
SINTEF Materials and Chemistry
N-7465 Trondheim, Norway

Lars O. Svaasand
Norwegian University of Science and Technology
Department of Electronics and Telecommunications
N-7491 Trondheim, Norway

Tore Lindmo
Norwegian University of Science and Technology
Department of Physics
N-7491 Trondheim, Norway

Abstract. We demonstrate low-coherence interferometry (LCI) for dye diffusion measurements in scattering tissue phantoms. The diffusion coefficient of a phthalocyanine dye in 1.5% agar gel containing scattering Intralipid was measured using a dual-wavelength interferometer. One wavelength was matched to the absorption peak of the dye at 675 nm. The other, 805 nm, was not affected by the dye, and was used to correct for varying sample scattering as a function of depth, assuming a constant ratio between scattering at the two wavelengths. The same wavelength dependence of scattering is assumed for the entire sample, but no *a priori* knowledge about the amount of scattering is needed. The dye diffusion coefficient was estimated by fitting a mathematical model of the interferometer signal to the measured LCI envelope. We compare results obtained using both a constant-scattering and a depth-resolved-scattering approach to determine the sample scattering. The presented method provides robust estimation of the diffusion coefficient when spatial resolution in determining the depth-resolved scattering is varied. Results indicate that the method is valid for samples having continuous spatial variations in the scattering coefficient over lengths as short as the coherence length of the probing light. The method allows *in situ* characterization of diffusion in scattering media. [DOI: 10.1117/1.2159000]

Paper 04229RR received Nov. 26, 2004; revised manuscript received Sep. 7, 2005; accepted for publication Sep. 16, 2005; published online Jan. 24, 2006.

1 Introduction

Since its introduction[1] optical coherence tomography (OCT) has become a well-established technique for obtaining high-resolution structural images of biological and other semitransparent tissue. The introduction of ultrabroadband spatially coherent sources[2,3] and full-field OCT instruments using affordable spatially incoherent white-light sources[4] has brought the resolution toward that obtained on histological sections. In recent years several groups have worked on expanding OCT to functional imaging. Promising results have been reported for Doppler flow imaging,[5] polarization sensitive OCT,[6] and spectroscopic OCT.[7–9] Several authors have addressed the challenge of extracting quantitative information on optical properties from scattering samples using low-coherence interferometry (LCI) and OCT. To obtain high precision in the estimated optical properties, knowledge is required about the relationship between optical properties of a scattering sample and the signal measured by LCI,[10–15] and about how speckle noise affects imaging of optical properties.[9,16,17]

The motivation for our work is to be able to monitor the concentration of photosensitizers used in photodynamic therapy (PDT). Apart from *in vivo* fluorescence monitoring, the photosensitizer part of *in vivo* PDT dosimetry is still in its infancy.[18] The requirement for *in situ*, noninvasive monitoring of drug concentration rules out methods that measure diffusion as a steady-state molecular mobility, and methods based on special measurement or sample geometries.[19] OCT represents a promising method to meet this challenge. Hand-held or endoscope-based OCT systems can access a variety of sites within the body and provide high-resolution cross-sectional images from which it is possible to determine the optical properties and thus the photosensitizer concentration and the effect of photosensitizer diffusion.

We have previously presented results from a first step toward the goal of noninvasive concentration monitoring by OCT, by measuring diffusion of a PDT-related dye in 1.5% agar gel.[20] A model of the OCT signal as a function of sample depth and time in the presence of a diffusing dye was then fitted to experimental data in order to obtain an estimate of the diffusion coefficient. The model assumed homogeneous samples having a constant scattering coefficient. The scattering coefficient of 1.5% agar gel was measured using OCT prior to the diffusion measurements, and found to be 0.06 mm^{-1} and thus one to two orders of magnitude below realistic values for the scattering coefficient of tissue. In the

Address all correspondence to Tore Lindmo, Norwegian University of Science and Technology, Department of Physics, N-7491 Trondheim, Norway. Tel.: +47 73 59 34 32; Fax: +47 73 59 86 84; E-mail: Tore.Lindmo@phys.ntnu.no

1083-3668/2006/11(1)/014017/9/$22.00 © 2006 SPIE

present work we further develop the method presented in Ref. 20 toward application on realistic tissue samples by performing measurements on agar samples having different amounts of Intralipid (IL) added to increase scattering. Measurements are done simultaneously at two wavelengths. One wavelength matches the absorption peak of the dye, and the other, which is unaffected by the dye, is used to determine the scattering coefficient of the samples, using a simple but realistic model for the relationship between scattering at the two wavelengths. An estimate of the diffusion coefficient is obtained using a more general version of the parameter-fitting approach presented in Ref. 20. The model of the LCI signal used in the present paper is extended to handle slow variations in the scattering coefficient with depth whereas the model used in Ref. 20 required a constant scattering coefficient known prior to the diffusion measurements. While presently only tested on samples having homogeneous scattering properties, this method should be suitable for diffusion measurements on real tissue where the scattering coefficient is generally a function of position.

Reported values for the scattering coefficient of biological tissue are in the range[10] $1-10\ \mathrm{mm}^{-1}$. We present results on samples having scattering coefficients up to $\approx 3\ \mathrm{mm}^{-1}$ thus lying within the range of realistic values for tissue scattering coefficients.

2 Model

The previous letter[20] gives a description of the model used to determine the diffusion coefficient of a dye which diffuses into a gel. We showed that the logarithm of the interference signal envelope, $A_\lambda(z,t)$ recorded at wavelength λ, can be expressed as a function of the depth- (z) and time-resolved (t) attenuation coefficient of the gel-dye sample, $\mu_{t\lambda}(z,t)$:

$$\ln[A_\lambda(z,t)] = \ln(|r_\lambda(z)|G_\lambda) - 2\int_0^z \frac{1}{2}\mu_{t\lambda}(z',t)dz' = \ln(|r_\lambda(z)|G_\lambda) - \int_0^z [\mu_{s,gel\lambda}(z') + \varepsilon_{a\lambda}C(z',t)]dz'. \quad (1)$$

The envelope, $A_\lambda(z,t)$, is proportional to the field of the light back-scattered from geometrical depth z in the sample.[21] Since the field is the square root of the intensity, the field attenuation coefficient is 1/2 the intensity-based attenuation coefficient μ_t while the factor 2 arises from double-pass of the light which probes the sample. G_λ is a constant which depends on the intensity of the incident light in the interferometer and gain factors in the detection system, $r_\lambda(z)$ is the average field reflectivity of the sample, $\mu_{t,gel,\lambda}(z)$ is the total attenuation coefficient of the Intralipid-containing agar gel, $\varepsilon_{a\lambda}$ is the extinction coefficient of the absorbing dye, and $C(z,t)$ is the depth- and time-dependent dye concentration. In Eq. (1) we assume that the Intralipid-containing agar gel has negligible absorption compared to scattering, and that the dye has negligible scattering compared to absorption. The scattering coefficient of a sample is related to its field reflectivity through the relation[22]

$$\mu_{s,\lambda}(z) \propto \langle |r_\lambda(z)|^2 \rangle. \quad (2)$$

When $\mu_{s,\lambda}(z)$ and thus $r_\lambda(z)$ is constant or slowly varying as a function of depth, the first term in Eq. (1) can be approximated by a constant. This approximation is used throughout the present work, and we define $K_\lambda \equiv \ln(|r_\lambda(z)|G_\lambda)$.

For the case where dye is distributed evenly on the surface of the gel at time $t=0$, over an area much larger than the diameter of the probing light beam, a good approximation for the dye concentration as a function of depth and time, is given by the one-dimensional delta-source solution of the diffusion equation for a semi-infinite medium:[23]

$$C(z,t) = \frac{M}{S\sqrt{\pi D t}} \exp\left[-\frac{z^2}{4Dt}\right] \quad (3)$$

where M is the total mass of dye deposited on the top surface area S of the gel.

Equations (1) and (3) constitute the model which we use for the interferometer signal. Measurements are carried out at two wavelengths where one (λ_1) is absorbed by the dye, and the other (λ_2) is not affected by the dye. An estimate of the diffusion coefficient, D, is determined by fitting of the model of Eqs. (1) and (3) to experimental data obtained at λ_1 using D, M, and K_λ as fitting parameters. In order to carry out the parameter fitting an estimate of the scattering coefficient at λ_1 is required. In the present work we use two approaches to estimating the scattering coefficient. The first approach assumes a constant scattering coefficient, while the second approach can be used for samples having a scattering coefficient which varies slowly as a function of sample position. Both methods are based on a single-scattering model of the LCI signal first used for estimating optical properties by Schmitt and Knüttel.[10] For samples where the LCI signal also is influenced by multiple scattering, the simple single-scattering model must be replaced by more advanced models taking the effect of multiple scattering into account.[21,24,25]

When λ_2 is unaffected by the dye, Eq. (1) is reduced to

$$\ln[A_{\lambda_2}(z,t)] = K_{\lambda_2} - \int_0^z \mu_{s,gel,\lambda_2}(z')dz', \quad (4)$$

which in the case of constant scattering is further simplified to

$$\ln[A_{\lambda_2}(z)] = K_{\lambda_2} - \mu_{s,gel,\lambda_2} \cdot z. \quad (5)$$

In this case linear regression on the logarithm of the recorded envelope can be used to find an estimate of the scattering coefficient of the gel, μ_{s,gel,λ_2}.

In tissue, the scattering coefficient is generally a function of position, and more complicated procedures must be used to estimate the scattering properties. In the present work we limit the study to samples having a slowly varying depth-dependent scattering. In this case, one approach to obtaining a depth-resolved estimate of the scattering coefficient is by spatially filtering and differentiating the logarithm of the recorded envelope:[9]

$$\hat{\mu}_{s,gel,\lambda_2}(z) = -\frac{d}{dz}\ln[A_{\lambda_2}(z) \otimes h_z(z)]. \quad (6)$$

Spatial filtering is necessary in order to reduce the large uncertainty in a depth-resolved estimate of the attenuation coefficient due to inherent speckle noise in an LCI signal. Following the approach of Ref. 9, we carry out the filtering by convolving the envelope with a filter function $h_z(z)$. The full width at half maximum of the filter function is denoted L_z and determines the spatial resolution of the depth-resolved attenuation-coefficient estimator. The symbol $\otimes$ denotes the convolution operation and the hat over the scattering coefficient indicates that it is an estimated value. Throughout this paper a Gaussian function truncated at $\pm 2\sigma$, where σ is the standard deviation of the Gaussian function, is used for the filter function. The Gaussian is a common filter function due to its lack of side lobes both in the position and spatial-frequency planes. Truncating it introduces some side lobes in the frequency plane but provides strict control over which parts of the filtered data that are influenced by edge effects. The properties and limitations of the attenuation coefficient estimator in Eq. (6), including its variance, is thoroughly discussed in Ref. 9.

Once the depth-resolved scattering coefficient at λ_2 is determined, the scattering coefficient at λ_1 can be estimated. In this paper we use a simple but realistic model of the scattering properties, assuming that there is a constant relationship between the scattering coefficient at the two wavelengths independent of Intralipid concentration and the presence of dye in the gel. Following a standard approach used by several authors,[26,27] we assume that there is a constant ratio between the scattering coefficient at the two wavelengths. We denote the ratio between the two scattering coefficients F:

$$F = \frac{\mu_{s,\lambda_1}}{\mu_{s,\lambda_2}}. \quad (7)$$

For samples having a more complicated relation between the scattering coefficient at the two wavelengths, more sophisticated approaches to separating the effects of scattering and absorption is required. Recently Yang et al.[28] proposed a novel method based on spectral triangulation for determining the absorption properties in a scattering sample without any *a priori* knowledge of wavelength dependence of the scattering properties. This is achieved by using a third wavelength, and assuming a linear, but unknown, relationship between scattering at the three wavelengths. Another novel method for separating absorption from scattering was presented by Xu et al.[15] They analyzed the spectrum of an OCT signal recorded using a broad-bandwidth source as a function of depth and separated the spectrum change due to absorption and scattering using a least squares fitting algorithm.

The model for the LCI signal from a sample containing a diffusing dye described above assumes that the diffusion coefficient does not vary as a function of position in the sample. It should be possible to extend the model in order to include variations in the diffusion coefficient as a function of the sample scattering, but this is beyond the scope of the present study and requires more knowledge about dye diffusion in agar gel and the effect of Intralipid on the diffusion properties.

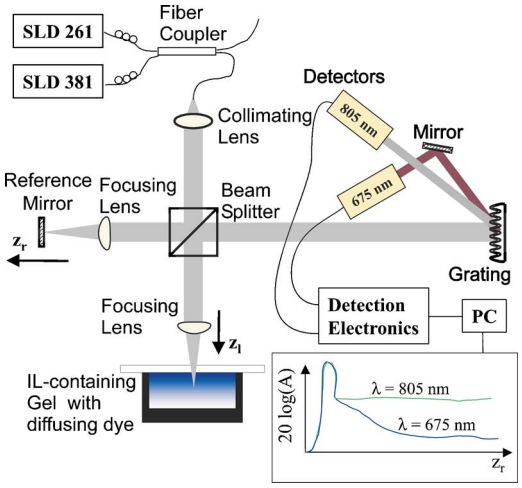

Fig. 1 Schematic illustration of the wavelength-multiplexed interferometer used for diffusion measurements. Light from two pigtailed SLDs having center wavelengths of $\lambda_1 = 675$ nm and $\lambda_2 = 805$ nm is multiplexed in a fiber coupler. Light from one of the fibers from the fiber coupler is launched into the free-space Michelson interferometer through a collimating lens. Depth scanning is obtained by adjusting the position (z_r) of the reference mirror using a linear translation stage. Dynamic focus tracking is obtained by scanning the position (z_l) of the sample-arm focusing lens using another linear translation stage (see text). A ruled gold grating is used for wavelength demultiplexing, and light from the two sources is recorded by separate detectors.

3 Experimental Setup

For the measurements, we use a bulk Michelson interferometer, as shown in Fig. 1. Light from two pigtailed superluminescent diodes from Superlum Diodes is multiplexed in a fiber coupler before it is launched into the free-space interferometer through a collimating lens. According to data from the manufacturer, the diodes have center wavelengths 675 and 805 nm, and spectral FWHMs 10 and 18 nm, respectively. We have measured the coherence lengths in air to be $l_c = 18.1$ μm for the 675-nm source and $l_c = 14.2$ μm for the 805-nm source. The coherence lengths in a sample are found by dividing the coherence lengths in air by the group refractive index of the sample. These coherence lengths correspond to spectral FWHM 11 and 20 nm for the 675- and 805-nm source, respectively, assuming Gaussian spectra. The power at the interferometer input was measured to 0.4 and 0.8 mW for the 675- and 805-nm source, respectively. The light is focused into the sample by a focusing lens having focal length $f = 14.5$ mm (Melles Griot 06GLC003). An identical lens is used in front of the reference mirror in order to match dispersion in the two interferometer arms. We use focus tracking[29] to ensure that the focus of the probing beam overlaps with the coherence volume of the interferometer. The focusing lens is scanned along with the reference mirror using lens velocity $v_l = v_r/n_g^2$, where v_r is the velocity of the reference mirror and n_g is the group refractive index of the sample. Linear translation stages are used for scanning of the focusing lens and reference mirror. Between each A-scan the sample was displaced transversally using a third linear translation stage. For all the experiments presented, the reference-mirror scanning velocity was $v_r = 1$ mm/s and the transversal distance between each A-scan was 10 μm. Demultiplexing is carried out

using a ruled gold grating, and the envelope of the interferometer signal is recorded simultaneously at both wavelengths. The system has a dynamic range of 90 dB.

4 Tissue Phantoms

We have studied diffusion of aluminum phthalocyanine tetrasulfonate chloride dye (AlPcS834, Porphyrin Products, Inc.) in 1.5% agar gel containing various amounts of scattering Intralipid. The dye has molecular weight MW =895.19 Daltons. It has high solubility in water and is thus not expected to be present in the IL phase of the samples. Using a commercial absorption spectrometer (Agilent 8452 UV-Visible Spectrophotometer), we measured the dye extinction coefficient at 675 nm to be $\varepsilon_{a,675}=44$ ml/mg·mm, about three orders of magnitude larger than at 805 nm. Thus with $\lambda_1=675$ nm and $\lambda_2=805$ nm, the equations in Sec. 2 are valid.

Prior to the diffusion measurements, initial LCI measurements were carried out at both wavelengths on agar gels having different concentrations of Intralipid and no absorbing dye. The scattering coefficient of the agar-IL samples was determined using linear regression on the logarithm of the recorded interferometer envelope. Based on these initial measurements the value of F, defined in Eq. (7), was found to be 1.5 ± 0.05 over a wide range of Intralipid concentrations.

5 Experimental Method

Agar-gel samples having Intralipid concentrations $C_{IL}=0.15\%$ and $C_{IL}=0.30\%$ were prepared in 10-mm-deep cylindrical cuvettes having inner diameter 18 mm. In this first demonstration of diffusion measurements on scattering samples, we wanted to limit the variation in the scattering coefficient and chose to prepare samples having only two different predefined Intralipid concentrations. A concentration of $C_{IL}=0.30\%$ in agar gel resulted in a scattering coefficient of ≈ 3 mm^{-1}, and we found this to be the highest practical scattering coefficient for the given dynamic range of our system.

For convenience we prepared a stock solution of dissolved dye having a concentration of 4 mg/ml. Using a micro pipette 20 μl of the stock solution was deposited onto the gel, distributing the solution as evenly as possible. Details on the choice of amount of deposited dye is given below. For each agar-IL sample, the dye was deposited 30 min after sample preparation. After depositing the dye, the cuvette was covered with a glass slide, and placed in the sample arm of the interferometer. The LCI envelope was recorded as a function of depth and time at both wavelengths. For each sample, measurement started immediately after deposition of the dye, acquiring a series of 40 A-scans over a time period of about 2.5 min. The sample was displaced 10 μm transversally between each A-scan in order to obtain A-scans having decorrelated speckles, and thus enable speckle averaging. To study the time development due to diffusion, data series at the same transversal positions on the sample were also acquired at three later time points. Thus, a total of four data series were recorded during 30 min after dye-deposition for each of the agar samples. The depth information was converted from optical depth to geometrical depth, z, using $n=1.34$ for the refractive index.

At 675 nm back-scattering just underneath the surface of the Intralipid-containing agar gel gives an LCI signal about 30 dB above the instrument noise level. The signal decreases due to scattering and absorption as we probe into the sample. For the model in Eqs. (1) and (3) to be valid, care must be taken that the signal is well above the noise level of the instrument throughout the probing depth. The amount of dye deposited on the sample surface and the amount of scattering thus limits the maximum probing depth. When designing the experiments, we determined the approximate maximum probing depth for each level of sample scattering by finding the depth where signal reduction due to scattering alone was approximately 10–15 dB compared to the signal level at the sample surface. By trial we then determined the amount of deposited dye that would reduce the signal further due to absorption to about 5 dB above the noise level at the maximum probing depth. Following this procedure signal reductions due to scattering and absorption were about equal.

6 Experimental Results and Discussion

Depth- and time-resolved data sets were recorded from diffusion measurements using 19 samples having an Intralipid concentration of $C_{IL}=0.15\%$, and 8 samples having $C_{IL}=0.30\%$ following the procedure outlined above. The diffusion measurements are time consuming, and the series of measurements on 0.30%-IL samples was terminated after 8 parallel samples were measured. The difference in number of samples is taken into account in the statistical analysis of the experimental results.

Figure 2 shows gray-scale images of the logarithm of the LCI envelope from one of the $C_{IL}=0.15\%$-samples recorded at both wavelengths and plotted as a function of geometrical depth and time. In the plot t and z correspond to t and z in Eq. (3). The black areas in the images correspond to time periods in which no data was acquired. In the image recorded at 805 nm the average envelope is constant as a function of time whereas the image recorded at 675 nm shows a time development: Shortly after dye deposition the backscattered intensity falls rapidly as a function of imaging depth due to a high dye concentration near the glass-gel interface. Later, diffusion of the dye into the gel results in lower concentration levels and a slower decrease in backscattered intensity with depth.

Data in each of the four series were averaged transversally, resulting in depth-resolved speckle-averaged envelopes recorded at four different times for each of the two wavelengths. In order to obtain an estimate of the diffusion coefficient, the model in Eqs. (1) and (3) was fitted to the logarithm of the speckle-averaged LCI envelope at 675 nm, with D, M, and K as fitting parameters, using a least-squares algorithm. The data recorded at 805 nm was used to find an estimate of the sample scattering coefficient prior to fitting.

As described in Sec. 2, we used two approaches for estimating the scattering coefficient, and parameter fitting was carried out using both approaches for all recorded data sets. For the first approach we assumed constant scattering as a function of depth, and used linear regression on the logarithm of the averaged envelope recorded at 805 nm, to obtain an estimate of the gel-IL scattering coefficient, $\mu_{s,805,gel}$, as described in relation to Eq. (5). Using Eq. (7) we thus found an estimate of $\mu_{s,675,gel}$, the scattering coefficient at 675 nm, and

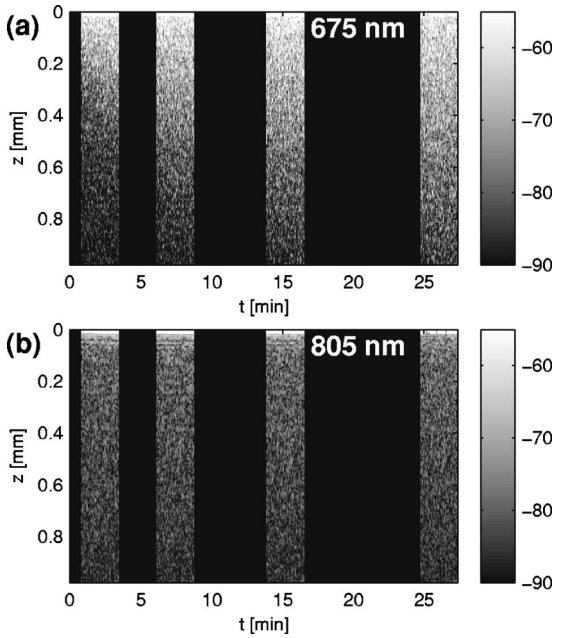

Fig. 2 Gray-scale images showing the logarithm of the interferometer envelope of four series of A-scans recorded from the same 0.4 ×1.0 mm vertical section of an Agar sample having Intralipid concentration C_{IL}=0.15%. The abscissa represents the time t after dye deposition, and the ordinate axis is the geometrical depth in the sample, where z=0 is the glass-gel interface. Panels (a) and (b) show data recorded at wavelengths 675 and 805 nm, respectively. The black areas in the plots represent time periods where no data is acquired.

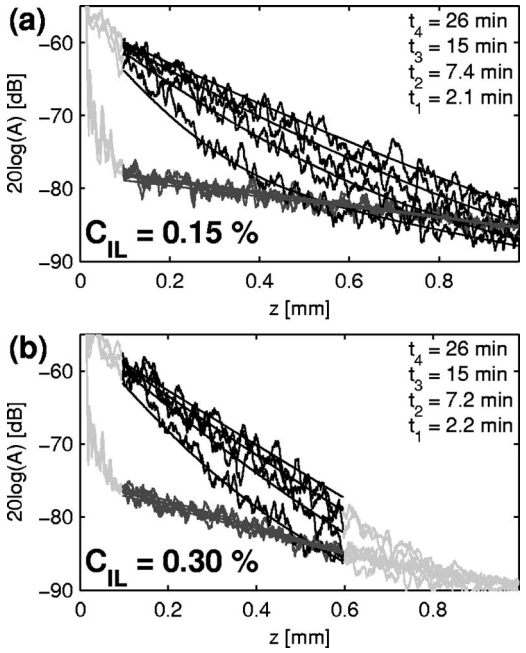

Fig. 3 Typical experimental data plotted together with fitted model based on estimating the scattering coefficient as a constant, using the constant-scattering approach. Speckle-averaged LCI envelopes are plotted as a function of depth for each of the four time series (t_1–t_4) obtained from two samples having Intralipid concentration C_{IL} =0.15% [panel (a)] and C_{IL}=0.30% [panel (b)]. The jagged curves are experimental data recorded at 675 and 805 nm. To avoid influence from the noise level (at −90 dB) and the reflection from the glass-gel interface (at z=0), data in a limited depth interval is used for parameter fitting, as described in Sec. 5. The experimental data within this interval is plotted in black and dark gray for 675 nm and 805 nm, respectively, while the experimental data outside this interval is plotted using light gray. The mean time after dye deposition for each of the curves is t_1 (bottom 675-nm curve) to t_4 (top 675-nm curve). The smooth black lines show the fitted model of Eqs. (1) and (3) for 675 nm. For the model plotted in this figure, the scattering coefficient at 675 nm was assumed constant, and was determined from the envelope recorded at 805 nm using the constant-scattering approach. For 805 nm the linear regression lines are plotted in dark-grey together with the experimental data.

used this value as a constant parameter in Eq. (1). We denote this the constant-scattering approach. In the second approach, which we denote the function-of-depth approach, we allow depth-dependent scattering and use Eqs. (6) and (7) to find a depth-resolved estimate of the scattering coefficient at 675 nm which then is used in Eq. (1). Since the samples in the present work are relatively homogeneous, we expect similar values for the diffusion coefficient for the two approaches.

6.1 *Assuming Constant Scattering*

Figure 3 shows speckle-averaged LCI envelopes from two typical data sets recorded at both wavelengths on samples prepared using the two different predefined Intralipid concentrations. The constant-scattering approach to estimating the scattering coefficient was used, and a value for the scattering coefficient at 805 nm was obtained from the slope of the regression line of the logarithm of the envelope recorded at 805 nm. Both the regression lines and the logarithm of the 805-nm envelope are plotted in the figure. For each sample we used the average of the scattering coefficient obtained from all four data series as an estimate for $\mu_{s,gel,805}$. Model fitting was carried out on the data set recorded at 675 nm using the constant value for $\mu_{s,gel,675}$, obtained from $\mu_{s,gel,805}$ for each sample. Figure 3 shows the fitted model for the LCI signal at 675 nm as well as experimental data. For both IL concentrations there is good agreement between experimental data and the fitted model.

Results from n=19 samples having C_{IL}=0.15% and n=8 samples having C_{IL}=0.30% are summarized in Table 1. Also presented in the table are 95% confidence intervals for the diffusion coefficient based on results from the two series. For the constant-scattering approach we obtain 95% confidence intervals of $D=(2.1\pm0.15)\times10^{-10}$ m^2/s and $D=(3.1\pm0.80)\times10^{-10}$ m^2/s for samples having C_{IL}=0.15% and C_{IL}=0.30%, respectively. These two mean values are statistically different down to a 1.8% significance level. Combining the results from the two series of sample IL concentrations we obtain $D=(2.6\pm0.51)\times10^{-10}$ m^2/s as the mean value and standard deviation of the diffusion coefficient. At a 5% significance level this result is not statistically different from the result presented in our previous letter[20] obtained from measurements on agar without Intralipid, and thus having very low scattering.

6.2 *Allowing Depth-dependent Scattering*

As a first step toward using the method presented in this paper for estimating the diffusion coefficient of a dye diffusing in a sample having unknown, and possibly spatially varying, scat-

Table 1 Overview of the measurement results.

C_{IL} [%]	n	$\hat{\mu}_s$: method of estimation	L_z [μm]	$\langle D \rangle$ [10^{-10} m^2/s]	σ_D [10^{-10} m^2/s]	95% CI [10^{-10} m^2/s]	MSE [dB]
0.00	10	Støren et al.[20]	—	2.5	0.30	(2.5±0.20)	—
0.15	19	CS[a]	—	2.1	0.30	(2.1±0.15)	1.4
0.30	8	CS	—	3.1	0.98	(3.1±0.80)	1.8
0.15	19	FOD[b]	100	2.8	0.57	(2.8±0.27)	1.4
0.15	19	FOD	20	2.7	0.51	(2.7±0.24)	1.9
0.15	19	FOD	2	3.0	0.62	(3.0±0.30)	3.2
0.30	8	FOD	100	3.8	1.0	(3.8±0.84)	1.7
0.30	8	FOD	20	3.7	1.3	(3.7±1.04)	2.5
0.30	8	FOD	2	3.8	1.5	(3.8±1.20)	3.5

[a] $\hat{\mu}_s$ determined using the constant-scattering approach.
[b] $\hat{\mu}_s$ determined using the function-of-depth approach.

tering, we used the function-of-depth approach described in Sec. 5 on the relatively homogeneous agar-IL samples. Prior to the diffusion measurements we suspected that there could be local variations in the scattering coefficient of the samples due to a nonperfect distribution of Intralipid in the agar gel. The objective of this analysis was to test the feasibility of the function-of-depth approach to estimating the scattering properties, thus allowing local variations in scattering properties.

Figures 4 and 5 show the same experimental data as Fig. 3. In Fig. 6 the experimental data at 805 nm is omitted from the figure for clarity. All three figures show the fitted model for the LCI signal at 675 nm where $\mu_{s,gel,675}(z)$ is determined from the depth-resolved estimate of $\mu_{s,gel,805}(z)$ obtained using Eq. (6). In Figs. 4–6 filter lengths of $L_z=100$, 20, and 2 μm, respectively, are used in estimating the depth-resolved scattering coefficients. For each of the speckle-averaged envelopes at 675 nm the depth-resolved scattering coefficient obtained from the speckle-averaged depth scan at the corresponding time point recorded at 805 nm was used in Eq. (1).

For $L_z=100$ μm (Fig. 4) there is a good fit between the model and experimental data at 675 nm. The model follows some of the slow variations in the experimental data as a function of depth. This indicates that the agar-IL samples may have local variations in the scattering coefficient and that the function-of-depth approach is able to recognize these. It also indicates that the model of Eqs. (1) and (3) tolerates slow variations in the scattering coefficient of the samples under study. Average numerical results obtained from parameter fitting for all samples are summarized in Table 1. The average mean square errors (MSE) per sample point for all the samples, analyzed with $L_z=100$ μm, are $MSE_{015}=1.4$ dB and $MSE_{030}=1.7$ dB for samples having $C_{IL}=0.15$ and $C_{IL}=0.30\%$, respectively. These are about the same values as those obtained using the constant-scattering approach.

Reducing the filter width to 20 μm (Fig. 5) and 2 μm (Fig. 6) results in a fitted model that more and more resembles experimental data. Some of the local variations in the experimental data may seem to be reproduced by the model for both of these short filter lengths, and thus might be due to local variations in the scattering coefficient, but this may be coincidental. The MSE increases as the filter length decreases and is approximately doubled at $L_z=2$ μm compared to $L_z=100$ μm.

Table 1 shows that the average values for the diffusion coefficient using the function-of-depth approach are 20–30% higher than the values obtained using the constant-scattering approach. However, the differences between average diffusion coefficient values within the function-of-depth approach are less than 10% for the three filter widths. These results show that the function-of-depth approach is robust to changes in filter width when it comes to modeling the interference signal. Since the depth resolution in LCI equals the coherence length, it is reasonable to choose the filter length equal to the coherence length, which for $\lambda_1=675$ nm is $l_c=13.5$ μm in the sample.

When increasing the filter length beyond $L_z=100$ μm we have found that the standard deviation, σ_D, in the estimated diffusion coefficient increases with the filter length. We believe this to be a result of the decrease in the depth interval used for model fitting due to the filter-width increase rather than the increase in L_z itself.

In order to obtain an accurate determination of D, the effect of diffusion of the dye, i.e., the time development of the speckle-averaged LCI envelope, must be visible in the measurements. When the depth dependency of the averaged envelopes is dominated by scattering in the depth interval used for parameter fitting, we expect a lower accuracy in determining D than when dye absorption dominates the signal. This assumption is supported by the above-mentioned increase in σ_D and also by the difference in σ_D between the two concentration series. We see that the standard deviation is 2–3 times higher within the results from the $C_{IL}=0.30\%$ series compared to the $C_{IL}=0.15\%$ series. When we designed the experiments, our emphasis was on ensuring that the absorption and

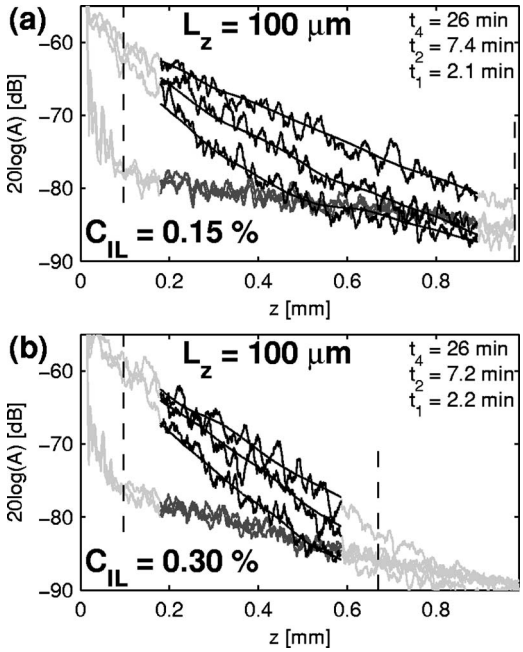

Fig. 4 Same experimental data as Fig. 3, but using the function-of-depth approach to estimate the scattering coefficient, which is allowed to depend on the position in the sample. Using Eqs. (6) and (7), a depth-resolved estimate for the scattering coefficient at 675 nm is obtained from the envelope recorded at 805 nm. A filter length of L_z=100 μm is used in the attenuation-coefficient estimator. For the transversally averaged A-scans at each time point, $\mu_{s,gel,675}(z)$ obtained from the corresponding averaged A-scans at 805 nm is then used in the model of Eqs. (1) and (3) for the LCI envelope at 675 nm. The smooth black lines show the fitted model plotted together with experimental data used in the parameter fitting procedure. Dashed vertical lines indicate the depth interval used for estimating the scattering coefficient. The part of the experimental data plotted using black and dark-gray lines indicate the part of the experimental data used for parameter fitting. The parameter-fitting interval is shorter than the estimation interval to avoid edge effects arising from the filtering described in Eq. (6). For clarity the experimental data and fitted model for the time t_3 are omitted from the figure, but data series recorded at all four time points were used in parameter fitting throughout the paper.

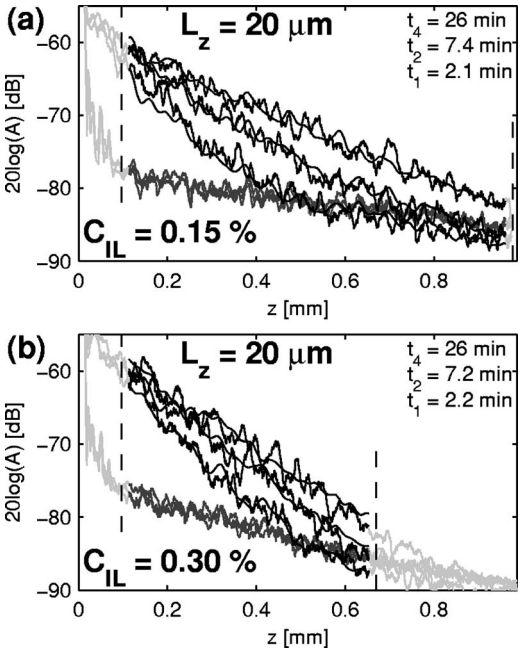

Fig. 5 Same as Fig. 4 but using filter length L_z=20 μm when estimating the scattering coefficient.

scattering contributed equally to the decrease in signal level at the maximum probing depth compared to the signal just below the sample surface. The probing depth was determined as the depth where scattering reduced the signal, in decibels, to about half of the dynamic range. This resulted in the same amount of dye being deposited for both IL-concentration series and thus the same absorption coefficient. The ratio of the scattering coefficient to the absorption coefficient is thus doubled from the C_{IL}=0.15% series to the C_{IL}=0.30% series. This may explain the larger σ_D for the latter series compared to the former.

It is worth noting that the increase in diffusion coefficient with Intralipid concentration which was commented in Sec. 6.1 is also seen when the data are analyzed using the function-of-depth approach. At the present time we do not understand the cause of this increase. Further studies of this effect should be carried out, but it is beyond the scope of the present paper.

7 Conclusion

The present work has demonstrated how the diffusion coefficient of a dye diffusing into a gel having unknown scattering properties may be determined using dual-wavelength LCI measurements. The method is based on simultaneous measurements at the two probing wavelengths where one is unaffected by the presence of the dye, and the other strongly absorbed by the dye.

The diffusion coefficient, D, is determined by fitting a mathematical model of the LCI envelope to the envelope recorded at the wavelength absorbed by the diffusing dye, using D as one of the fitting parameters. Measurement at the other wavelength, which is unaffected by the dye, is used for estimating the scattering coefficient at the absorbed wavelength. Two approaches to estimating the scattering properties, the constant-scattering approach and the function-of-depth approach, were tested. The first approach assumes homogeneous scattering properties while the second also can handle slow variations in scattering properties as a function of depth using a depth-resolved attenuation coefficient estimator previously presented by Støren et al.[9] As expected, the two approaches gave similar estimates of the diffusion coefficient for the samples used in the present work, namely agar gel having various concentrations of Intralipid added to increase scattering. The numerical value of the estimated diffusion coefficient was also found to be in reasonable agreement with a previously published value obtained from measurements on agar without Intralipid. The numerical values for the average diffusion coefficient determined from measurements on samples having two different Intralipid concentrations and using the two approaches to determine the scattering coefficient were in the interval $\langle D\rangle=[2.1,3.8]\times 10^{-10}$ m^2/s.

The estimate of D obtained using the function-of-depth approach to determine sample scattering was, for these rela-

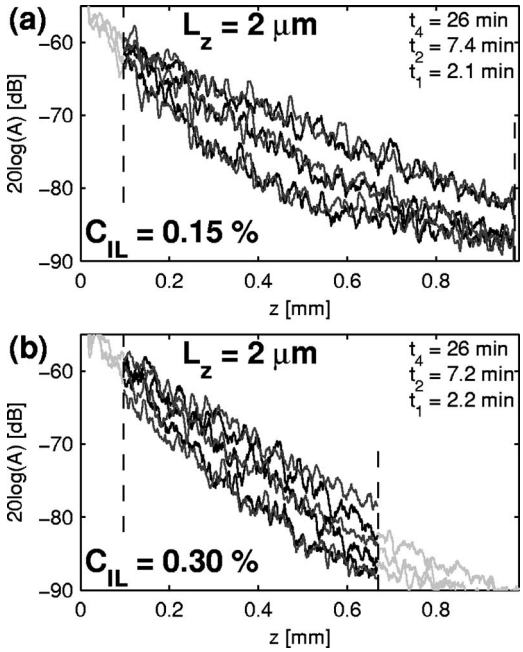

Fig. 6 Same as Fig. 4 but using filter length L_z=2 μm when estimating the scattering coefficient. The black curves are experimental data recorded at 675 nm while the dark-gray curves represent the fitted model. The statistical variations in the fitted model arise from fluctuations in the depth-resolved estimated scattering coefficient obtained from the data set recorded at 805 nm. For clarity the experimental data recorded at 805 nm have, however, been omitted from the figure.

tively homogeneous samples, found to be robust to changes in filter length (L_z) in the attenuation coefficient estimator. Spatial filtering is required when estimating the scattering coefficient based on LCI measurements due to inherent speckle noise in the measurements, and L_z limits spatial resolution in the depth-resolved estimate of the scattering coefficient. Filter lengths as short as 15% of the coherence length (l_c) in the samples were tested, and no significant deviations from the value of D obtained using longer filter lengths were found. A reasonable choice of filter length is thus L_z=l_c, since l_c limits spatial resolution in an LCI measurement. We expect the method to give reliable results also for samples having depth-dependent scattering, as long as the diffusion coefficient is relatively independent of scattering. Nevertheless further studies involving measurements using animal models or preferably measurements of dye diffusion in real PDT scenarios are necessary in order to verify that the presented method can be used for *in situ* monitoring of photosensitizer concentration in PDT.

The model of the LCI envelope used in the present work is only valid for slow variations in the scattering coefficient and must be modified if the method is to be used on samples or tissue having large, or discontinuous, variations in scattering as a function of depth.

Acknowledgments

This work is supported by project 111737/432 and 129104/420 financed by the Research Council of Norway. The authors wish to thank Prof. Ole J. Løkberg for helpful discussions on instrumentation.

References

1. D. Huang, E. A. Swanson, C. P. Lin, J. S. Schuman, W. G. Stinson, W. Chang, M. R. Hee, T. Flotte, K. Gregory, C. A. Pulifito, and J. G. Fujimoto, "Optical coherence tomography," *Science* **254**, 1178–1181 (1991).
2. J. G. Fujimoto, C. Pitris, S. Boppart, and M. Brezinski, "Optical coherence tomography, an emerging technology for biomedical imaging and optical biopsy," *Neoplasia* **2**, 9–25 (2000).
3. W. Drexler, "Ultrahigh-resolution optical coherence tomography," *J. Biomed. Opt.* **9**, 47–74 (2004).
4. A. Dubois, K. Grieve, G. Moneron, R. Lecaque, L. Vabre, and C. Boccara, "Ultrahigh-resolution full-field optical coherence tomography," *Appl. Opt.* **43**, 2874–2883 (2004).
5. Z. Chen, T. Milner, S. Srinivas, X. Wang, A. Malekafzali, M. van Gemert, and J. Nelson, "Non-invasive imaging of *in vivo* blood flow velocity using optical Doppler tomography," *Opt. Lett.* **22**, 1–3 (1997).
6. J. de Boer, T. Milner, M. van Gemert, and J. Nelson, "Two dimensional birefringence imaging in biological tissue by polarisation sensitive optical coherence tomography," *Opt. Lett.* **22**, 934–936 (1997).
7. J. Schmitt, S. Xiang, and K. Yung, "Differential absorption imaging with optical coherence tomography," *J. Opt. Soc. Am. A* **15**, 2288–2296 (1998).
8. U. Morgner, W. Drexler, F. Kärtner, X. Li, C. Pitris, E. Ippen, and J. Fujimoto, "Spectroscopic optical coherence tomography," *Opt. Lett.* **25**, 111–113 (2000).
9. T. Støren, A. Røyset, L. O. Svaasand, and T. Lindmo, "Functional imaging of dye concentration in tissue phantoms by spectroscopic optical coherence tomography," *J. Biomed. Opt.* **10**, 024037 (2005).
10. J. M. Schmitt, A. Knüttel, and R. F. Bonner, "Measurement of optical properties of biological tissues by low-coherence interferometry," *Appl. Opt.* **32**, 6032–6042 (1993).
11. Y. Pan, R. Birngruber, J. Rosperich, and R. Engelhardt, "Low-coherence optical tomography in turbid tissue: theoretical analysis," *Appl. Opt.* **34**, 6564–6574 (1995).
12. S. R. Thurber, A. M. Brodsky, and L. W. Burgess, "Characterization of random media by low-coherence interferometry," *Appl. Spectrosc.* **54**, 1506–1514 (2000).
13. L. Thrane, M. H. Frosz, T. M. Jørgensen, A. Tycho, H. T. Yura, and P. E. Andersen, "Extraction of optical scattering parameters and attenuation compensation in optical coherence tomography images of multilayered tissue structures," *Opt. Lett.* **29**, 1641–1643 (2004).
14. D. J. Faber, F. J. van der Meer, M. C. G. Aalders, and T. G. van Leeuwen, "Quantitative measurement of attenuation coefficients of weakly scattering media using optical coherence tomography," *Opt. Express* **12**, 4353–4365 (2004).
15. C. Xu, D. L. Marks, M. N. Do, and S. A. Boppart, "Separation of absorption and scattering profiles in spectroscopic optical coherence tomography using a least-squares algorithm," *Opt. Express* **12**, 4790–4803 (2004).
16. A. I. Kholodnykh, I. Y. Petrova, K. V. Larin, M. Motamedi, and R. O. Esenaliev, "Precision of measurement of tissue optical properties with optical coherence tomography," *Appl. Opt.* **42**, 3027–3037 (2003).
17. M. Pircher, E. Götzinger, R. Leitgeb, A. F. Fercher, and C. K. Hitzenberger, "Speckle reduction in optical coherence tomography by frequency compounding," *J. Biomed. Opt.* **8**, 565–569 (2003).
18. W. Star, "Light dosimetry *in vivo*," *Phys. Med. Biol.* **42**, 763–787 (1997).
19. B. Westrin, A. Axelsson, and G. Zacchi, "Diffusion measurements in gels," *J. Controlled Release* **30**, 189–199 (1994).
20. T. Støren, A. Simonsen, O. Løkberg, T. Lindmo, L. Svaasand, and A. Røyset, "Measurement of dye diffusion in agar gel by use of low-coherence interferometry," *Opt. Lett.* **28**, 1215–1217 (2003).
21. J. M. Schmitt and A. Knüttel, "Model of optical coherence tomography of heterogeneous tissue," *J. Opt. Soc. Am. A* **14**, 1231–1242 (1997).
22. A. Ishimaru, *Wave Propagation and Scattering in Random Media*, Vol. **2**, Academic Press, New York (1978).
23. J. Crank, *The Mathematics of Diffusion*, 2nd ed., pp. 11–16, Oxford University Press, New York (1976).
24. Y. Pan, R. Birngruber, and R. Engelhardt, "Contrast limits of coherence-gated imaging in scattering media," *Appl. Opt.* **36**, 2979–2983 (1997).
25. P. E. Andersen, L. Thrane, H. T. Yura, A. Tycho, T. M. Jørgensen,

and M. H. Frosz, "Advanced modelling of optical coherence tomography systems," *Phys. Med. Biol.* **49**, 1307–1327 (2004).
26. Y. Pan and D. L. Farkas, "Noninvasive imaging of living human skin with dual-wavelength optical coherence tomography in two and three dimensions," *J. Biomed. Opt.* **3**, 446–454 (1998).
27. U. Sathyam, B. Colston, L. DaSilva, and M. Everett, "Evaluation of optical coherence quantitation of analytes in turbid media by use of two wavelengths," *Appl. Opt.* **38**, 2097–2104 (1999).
28. C. Yang, L. E. L. McGuckin, J. D. Simon, M. A. Choma, B. E. Applegate, and J. A. Izatt, "Spectral triangulation molecular contrast optical coherence tomography with indocyanine green as the contrast agent," *Opt. Lett.* **29**, 2016–2018 (2004).
29. Z. Chen, T. Milner, and J. Nelson, "Optical Doppler tomographic imaging of fluid flow velocity in highly scattering media," *Opt. Lett.* **22**, 64–66 (1997).